Geophysical Research Letters

Supporting Information for

Preferential Summer Melt of Deeper Ridge Keels in the Central Arctic Ocean from Multibeam Sonar Data

E. Salganik[1,2], B. A. Lange[2,3], C. Katlein[4], I. Matero[4,5], P. Anhaus[4], M. Muilwijk[2], K. V. Høyland[1], and M. A. Granskog[2]

[1]Norwegian University of Science and Technology, Trondheim, Norway

[2]Norwegian Polar Institute, Fram Centre, Tromsø, Norway

[3]Norwegian Geotechnical Institute, Oslo, Norway

[4]Alfred-Wegener-Institut Helmholtz-Zentrum für Polar- und Meeresforschung, Bremerhaven, Germany

[5]Svalbard Integrated Arctic Earth Observing System Knowledge Centre, Longyearbyen, Svalbard

Contents of this file

Introduction

The supporting information presented here includes details of ocean heat flux calculations (Section S1), ancillary details about the ridge drilling profiles (Figure S1), ridge multibeam sonar surveys (Figure S2), comparison of data from drilling, sonar, and temperature buoy (Figure S3), evolution of physical parameters of first-year ice at the coring site (Figure S4), evolution of physical parameters of bottom parts of first-year ice and ridge (Figure S5), and estimates of ocean heat flux (Figure S6).

Text S1. Ocean Heat Flux Calculations

The amount of melted ice h_i depends on the sum of the conductive heat flux q_c and the ocean heat flux q_w and can be expressed as

$$-\rho_{si} L_{si} \, \partial h_i / \partial t = q_c + q_w, \quad (1)$$

where ρ_{si} is the sea-ice density, L_{si} is the effective latent heat of sea ice, and t is the time.

The conductive heat flux q_c depends on the temperature profile at the ice-water interface. During the investigated period from June 24 to July 21, both level ice and ridges were nearly isothermal, so the conductive heat flux q_c was assumed to be zero in our calculations. The sea-ice density ρ_{si} and the effective latent heat of sea ice L_{si} depend on the sea-ice salinity S_i, temperature T, and gas volume fraction v_g. For both first-year ice (FYI) coring site and Jaridge, these parameters were measured in situ. The results of our estimates are presented in Figure S5. The average ridge sea-ice density and the effective latent heat were equivalent to the values for sea ice with salinity of 2.6 and gas volume of 1.7%, identical to the average salinity of FYI during melt season and FYI average gas volume prior to melt season.

The average FYI density and the effective latent heat were corresponding to 15% less energy required to melt a unit volume of sea ice. This 15% difference was mainly caused by the presence of under-ice meltwater layers, which led to the increase of first-year ice bottom temperature and brine volume. In our calculation of the ocean heat flux, we use the average sea-ice density (909.1 kg/m^3) and the effective latent heat (92% of the value for pure ice) as for sea ice with salinity of 2.6 and gas volume of 1.7%. The lower estimate of first-year ice effective latent heat was not used for the ocean heat flux calculations as the areal fraction of under-ice meltwater layers was estimated as 20% (Smith et al., 2022) and was not representative for the area of sonar surveys (Salganik et al., in press).

The sea-ice density was found from Leppäranta & Manninen (1988) as:

$$\rho_{si} = \left(1 - v_b - v_g\right)\rho_i + v_b\rho_b, \quad (2)$$

The sea-ice brine mass fraction can be found from Notz (2005) as:

$$m_b = S_i/S_b \quad (3)$$

The sea-ice brine volume fraction can be found from Notz (2005) as:

$$v_b = 1 - v_g - \frac{1 - \frac{S_i}{S_b}}{1 + \frac{S_i}{S_b}\left(\frac{\rho_i}{\rho_b} - 1\right)} \quad (4)$$

The density of pure ice can be found from Pounder (1966) as:

$$\rho_i = 916.8 - 0.1403 \cdot T \quad (5)$$

The brine salinity can be found from Feistel & Hagen (1998) as:

$$S_b = -\mathrm{T}(17.5967 + 2.00661(-T)^{0.5} + 1.12533 \cdot T) \quad (6)$$

The brine density can be found from Schwerdtfeger (1963) as:

$$\rho_b = 1000.3 + 0.78237 \cdot S_b + 2.8008 \cdot 10^{-4} \cdot S_b^2 \quad (7)$$

The effective latent heat of sea ice can be found from Schwerdtfeger (1963) as:

$$L_{si} = (1 - m_b)L_i, \quad (8)$$

where L_i is the latent heat of pure ice.

To estimate ocean heat fluxes from oceanographic measurements, we use the model from McPhee (1992)

$$q_w = \alpha_h\rho_w c_w u(T_\infty - T_b), \quad (9)$$

where α_h is the coefficient of turbulent transport (0.0095 from Notz et al., 2003), ρ_w and c_w are the density and heat capacity of seawater (Millero, 2010), u is the friction velocity (0.47 m s^{-1} from Fer et al., 2022), T_∞ and T_b are the water and ice-water interface temperatures.

References

Feistel, R., & Hagen, E. (1998). *A Gibbs thermodynamic potential of sea ice*. *Cold Regions Science and Technology* (Vol. 28). https://doi.org/10.1016/S0165-232X(98)00014-7

Fer, I., Baumann, T. M., Koenig, Z., Muilwijk, M., & Tippenhauer, S. (2022). Upper-Ocean Turbulence Structure and Ocean-Ice Drag Coefficient Estimates Using an Ascending Microstructure Profiler During the MOSAiC Drift. *Journal of Geophysical Research: Oceans*, *127*(9). https://doi.org/10.1029/2022JC018751

Leppäranta, M., & Manninen, T. (1988). *The brine and gas content of sea ice with attention to low salinities and high temperatures*. Helsinki, Finland: Finnish Institute of Marine Research. Retrieved from http://aquaticcommons.org/id/eprint/6760

McPhee, M. G. (1992). Turbulent heat flux in the upper ocean under sea ice. *Journal of Geophysical Research*, *97*(C4), 5365. https://doi.org/10.1029/92JC00239

Millero, F. J. (2010). Equation of State of Seawater. *Oceanography*, *23*(3), 18–33. https://doi.org/10.5670/oceanog.2010.21.COPYRIGHT

Notz, D. (2005). *Thermodynamic and fluid-dynamical processes in sea ice*. University of Cambridge. Retrieved from http://mpimet.mpg.de/fileadmin/staff/notzdirk/Notz_PhD_abstract.pdf

Notz, D., McPhee, M. G., Worster, M. G., Maykut, G. A., Schlünzen, K. H., & Eicken, H. (2003). Impact of underwater-ice evolution on Arctic summer sea ice. *Journal of Geophysical Research: Oceans*, *108*(7), 3223. https://doi.org/10.1029/2001jc001173

Pounder, E. R. (1966). The Physics of Ice. *American Journal of Physics*. https://doi.org/10.1119/1.1973537

Salganik, E., Katlein, C., Lange, B. A., Matero, I., Ruibo, L., Fong, A. A., et al. (2023). Temporal evolution of under-ice meltwaterlayersand false bottomsand their impact on summer Arctic sea ice mass balance. *Elementa: Science of the Anthropocene*, *in press*. https://doi.org/https://doi.org/10.31223/X5H37R

Schwerdtfeger, P. (1963). The Thermal Properties of Sea Ice. *Journal of Glaciology*, *4*(36), 789–807. https://doi.org/10.1017/S0022143000028379

Smith, M. M., von Albedyll, L., Raphael, I. A., Lange, B. A., Matero, I., Salganik, E., et al. (2022). Quantifying false bottoms and under-ice meltwater layers beneath Arctic summer sea ice with fine-scale observations. *Elementa: Science of the Anthropocene*, *10*(1). https://doi.org/10.1525/elementa.2021.000116

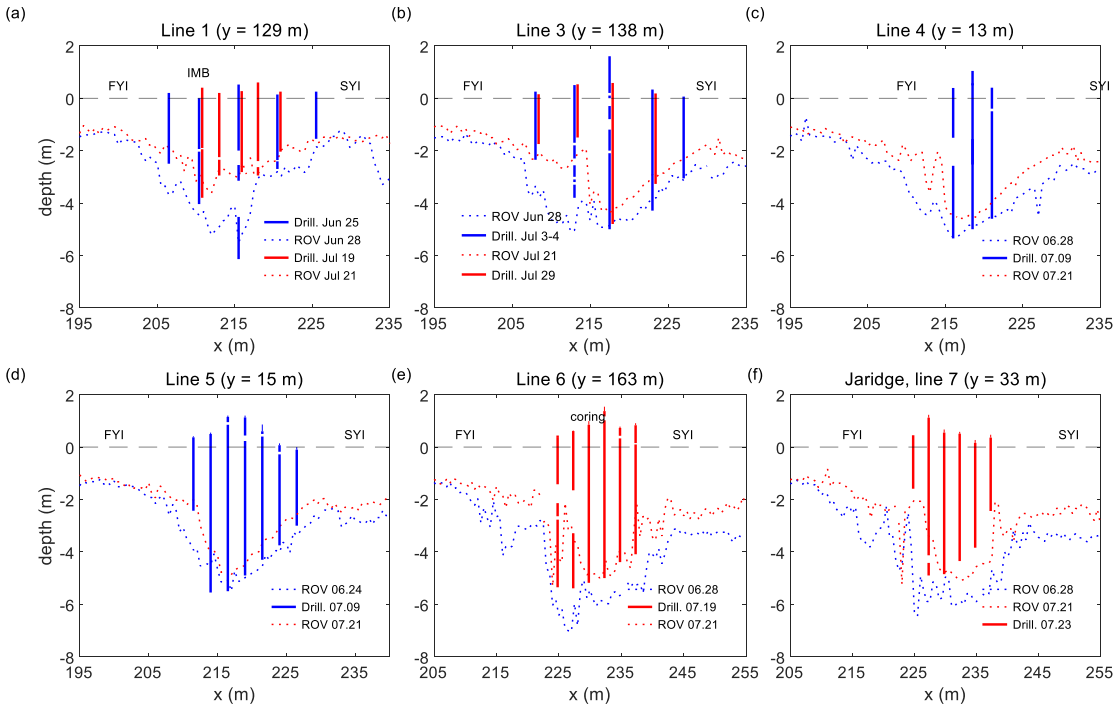

Figure S1. Ridge draft measurements from ROV multibeam sonar and ice drilling lines.

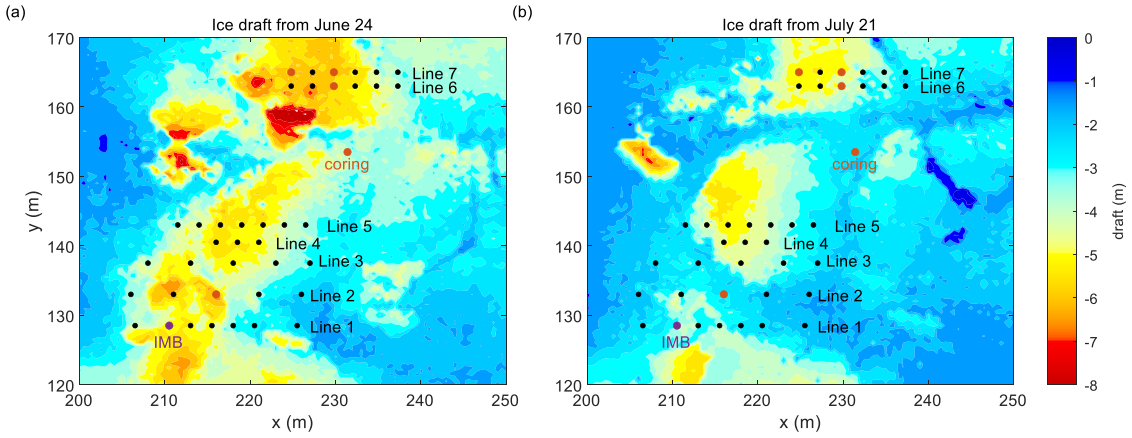

Figure S2. Contour plot with ice draft for June 24 (a) and July 21 (b). Black points show ridge drilling locations, purple point show the location of ice mass balance buoy (IMB), and red points show the location of ridge coring.

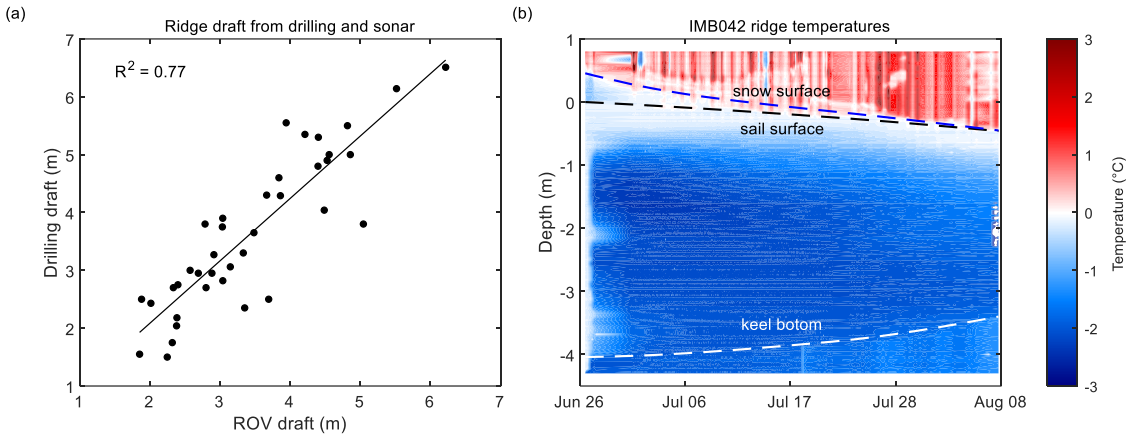

Figure S3. Comparison of ice draft from ROV multibeam sonar and manual drilling (a) and contour plot of the ridge temperature measurements from IMB042 buoy (b).

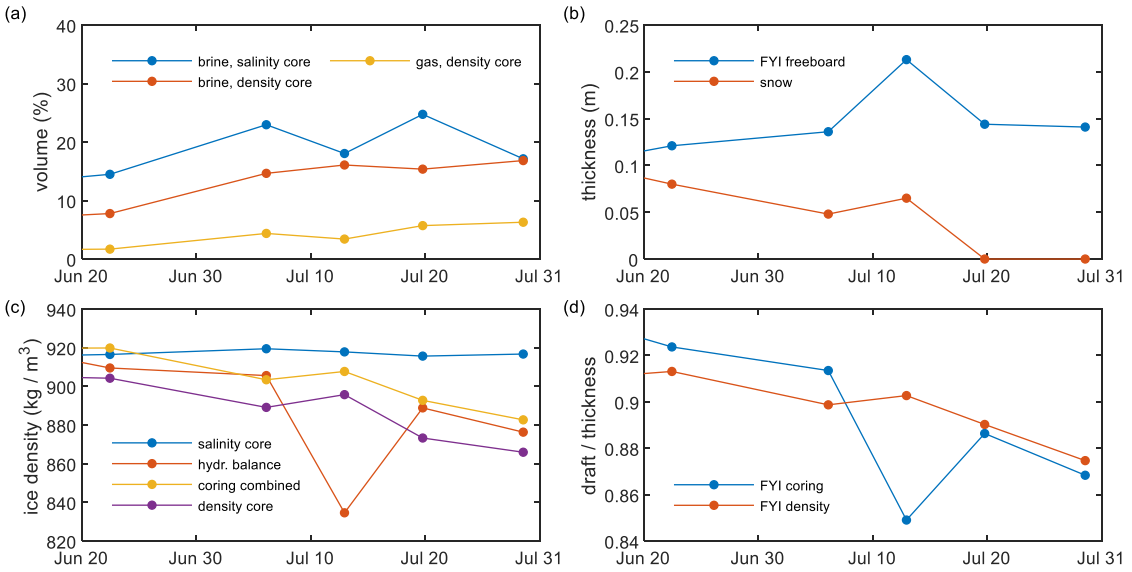

Figure S4. Evolution of brine and gas volume (a), snow and freeboard thickness (b), sea-ice density (c), and sea-ice draft and thickness ratio (d) measured or estimated from salinity and density cores at FYI coring site. Sea-ice density for combined salinity and density cores was calculated assuming gas volume from density core and brine volume

from salinity core. Sea-ice density for hydrostatic balance was estimated from the measured snow and ice thickness and draft.

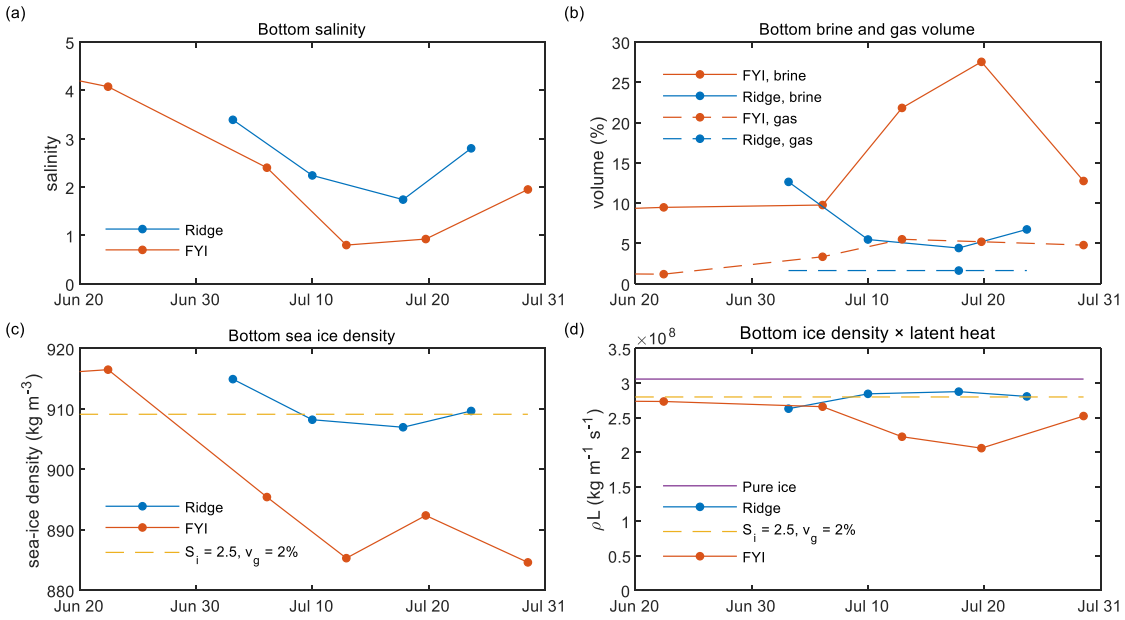

Figure S5. Evolution of bottom sea-ice salinity (a), brine and gas volume (b), sea-ice density (c), and ice density and latent heat product (d) measured or estimated from salinity and density cores for first-year ice (FYI) coring site and Jaridge. Bottom 0.20 m and 0.55 m of ice cores were used for FYI and ridge estimates, respectively.

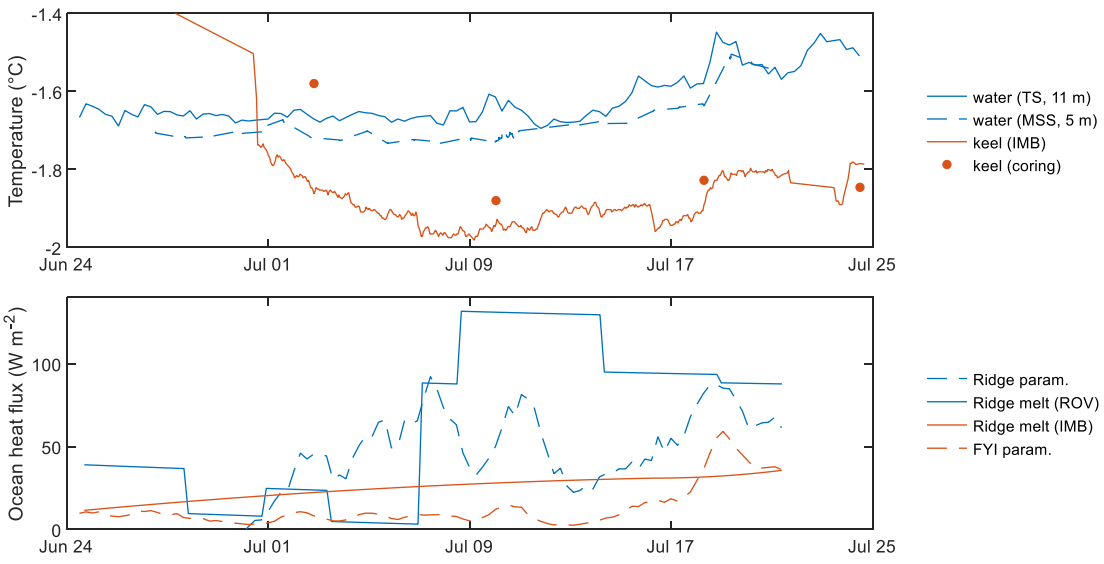

Figure S6. Temperature of Jaridge keel bottom from temperature buoy (IMB) and coring; and water temperature from the Polarstern thermosalinograph (TS) at 11-m depth and microstructure profiles (MSS) at 5-m depth (a), ocean heat flux estimated from ocean parameterization for the ridge, from ridge bottom melt estimates from ROV, from ridge

bottom melt estimates from ice mass balance buoy (IMB), and from ocean parameterization for FYI (b).